HEFAT2014
10th International Conference on Heat Transfer, Fluid Mechanics and Thermodynamics
14 – 16 July 2014
Orlando, Florida

EXPERIMENTAL ANALYSIS OF THE RATE OF ABSORPTION OF STEAM BUBBLES IN LITHIUM BROMIDE SOLUTION FOR USE IN AN ABSORPTION HEAT TRANSFORMER

Donnellan P.[a]*, Byrne E.[a], Lee W.[b], Cronin K.[a]
*Author for correspondence
[a]Department of Process and Chemical Engineering, University College Cork, Ireland
[b]MACSI, Department of Mathematics and Statistics, University of Limerick, Ireland

E-mail: p.donnellan@umail.ucc.ie

ABSTRACT

An experimental investigation is conducted into the absorption of steam bubbles in a concentrated lithium bromide solution. The aim of the work is to determine whether such bubble absorption may be advantageously utilised within the absorber column section of an absorption heat transformer system. A glass bubble column is constructed and a high speed camera is used to track the collapse of steam bubbles at different temperatures and solution concentrations. A simple ordinary differential equation model is developed which is capable of explaining 96% of the observed experimental variance. Very high mass transfer coefficients of ~0.012m/s are observed which indicates that this method of absorption may have significant advantages over alternative methods previously examined.

INTRODUCTION

Minimising energy wastage remains a very important issue in the process and chemical industries. In this context, there is an opportunity for the investigation of a range of suitable alternative technologies which allow for the more efficient and sustainable use of energy. Absorption heat transformers are one such system. They are closed cycle thermodynamic units which are capable of upgrading the temperature of waste heat energy so that it may be recycled within a plant, thus dramatically reducing primary energy requirements [1].

The principle of operation of certain absorption heat transformers is the absorption of low temperature steam into a lithium bromide solution at a higher temperature. It is this absorption which actually increases the temperature of the waste heat energy [2]. Currently, the vast majority of reports in the literature achieve this absorption through the use of horizontal or vertical falling film absorbers [3, 4]. While this is a well-established technology, it has several key drawbacks in comparison to the direct absorption of steam vapour bubbles in the solution by means of a bubble column, such as a much lower contact surface area per unit vapour and lower heat and mass transfer coefficients.

It has been demonstrated that conventional vertical falling film absorbers, in which the LiBr-H_2O solution is flowing vertically downwards and absorbing water vapour on the outside of tubes containing a coolant, can achieve mass transfer coefficients of ~$3.15x10^{-5}$m/s [5]. The performance of the absorber may be increased dramatically by utilising a spray absorber instead. In spray absorbers, the solution is atomized in a nozzle before being sprayed into a vessel filled with water vapour, and mass transfer coefficients of ~$6x10^{-5}$m/s have been reported for such units [6]. The mass transfer coefficient may be increased even further to approximately $2x10^{-4}$m/s if the solution is not atomized, but instead falls through the water vapour as a liquid film, primarily due to the increased liquid mixing achieved by the falling film [7]. This design may then be further improved by allowing the liquid film to enter the absorber in a conical shape, leading to mass transfer coefficients of up to $7x10^{-4}$m/s [8].

The most successful heat and mass transfer coefficients reported to date for absorbers have been achieved by bubble absorbers. In a bubble absorber, the vapour is simply bubbled into the bottom of a bubble column containing the desired absorbent. It has been demonstrated using numerical simulations that the absorption of NH_3 vapour into a NH_3-H_2O solution may achieve mass transfer coefficients of ~$1.15x10^{-3}$m/s and heat transfer coefficients of ~16000W/(m^2K) [9]. It has also been shown in a direct comparison that a bubble column allows more effective absorption of NH_3 into NH_3-H_2O solution compared to a conventional vertical falling film absorber [10].

From the above literature review, it can be seen that bubble absorbers have significant advantages over conventional falling film units. However to the authors' best knowledge no bubble absorber operating with LiBr-H_2O solution has yet been tested, even though this is the most commonly utilised working fluid in absorption heat transformers [11]. Thus this study attempts to experimentally monitor the absorption of a single steam bubble in a concentrated LiBr-H_2O solution. A simple model is also be developed which allows for the prediction of bubble behaviour during the absorption process.

NOMENCLATURE

A	Surface Area (m^2)
$A_{projected}$	Vertically projected bubble area (m^2)
C	Water concentration (mol/m^3)
C_D	Drag coefficient
c_p	Specific heat capacity (W/(kg.K))
D	Pipe Diameter (m)
D_{ab}	Mass diffusivity of water in LiBr-H_2O solution (m^2/s)
dt	Time interval between frames in high speed video (1/500 seconds)
F	Force (N)
g	Acceleration due to gravity (m/s^2)
H	Enthalpy (J)
h	Specific enthalpy (J/kg)
h_{pw}	Partial specific enthalpy of water in LiBr-H_2O solution (J/kg)
k	Thermal conductivity (W/(m·K))
m	Mass (kg)
n	Moles
P	Pressure (Pa)
P*	Vapour pressure (Pa)
P^v	Partial pressure (Pa)
Q	Rate of enthalpy flow (W)
R	Radius (m)
T	Temperature (K)
t	Time (s)
t_{50}	Time for the modelled bubble's volume to reduce by 50% (s)
u	Liquid velocity (m/s)
v	Velocity (m/s)
V	Volume (m^3)
x	Lithium Bromide mass fraction (kg/kg)
y	Volume fraction in the vapour phase (m^3/m^3)

Dimensionless Numbers

Re	Reynolds Number = $\rho_L v_b D/\mu_L$
Pr	Prandtl Number = $c_{pL}\mu_L/k_L$
Sc	Schmidt Number = $\mu_L/\rho_L D$
Pe	Peclet Number = RePr
Pe_m	Mass transfer Peclet Number = ReSc

Greek Symbols

α	Liquid side heat transfer coefficient ($W/(m^2K)$)
α_{therm}	Liquid thermal diffusivity = $k/(c_p\rho)$ (m^2/s)
β	Liquid side mass transfer coefficient (m/s)
ρ	Density (kg/m^3)
μ	Dynamic Viscosity (Ns/m^2)
τ	Dimensionless Time parameter (t/t_{50})
σ	Surface Tension (N/m)

Subscripts

abs	absorption
B	Buoyancy
b	bubble
D	Drag
H_2O	Water
i	Bubble-Liquid interface
L	Bulk Liquid
LiBr	Lithium Bromide
v	Vapour
vm	Virtual Mass (or added mass)

EXPERIMENTAL SET UP

The experimental bubble column consists of a 1m high, 10cm wide glass cylinder, bolted on to a stainless steel base plate. The cylinder is filled with approximately 32cm of aqueous lithium bromide, and the solution is maintained at a constant temperature by circulating it through a temperature controlled oil bath at a flowrate of 29mL/s. The oil bath is operated in on-off mode, controlled by a Honeywell UDC 3000 PID controller, and the solution is pumped from the oil bath back into the cylinder by means of a Watson Marlow 505S peristaltic pump.

Measurement of some solution properties is made difficult due to the high temperature and concentration of the LiBr-H_2O solution. The concentration of Lithium Bromide in solution is often measured using a refractometer [4], however no reference data relating the solution's refractive index to lithium bromide concentration at temperatures of interest in this research (~140˚C) could be located. Thus the buoyancy force exerted by the solution on a copper bob of known mass and volume is measured by suspending the copper mass in the solution contained within the oil bath from a mass balance (Precisa 3610 CD-FR) (positioned directly above the oil bath). Simultaneously the temperature of the oil bath is being recorded by means of a thermocouple connected to the temperature logging software being used (Pico Log R5). By using equation 1 and the measured temperature, the mass fraction of lithium bromide salt in the solution may be found using the LiBr-H_2O solution density correlation reported by [12].

$$\rho_L(T_L, x_L) = \frac{F_B}{gV_{CopperMass}} \quad (1)$$

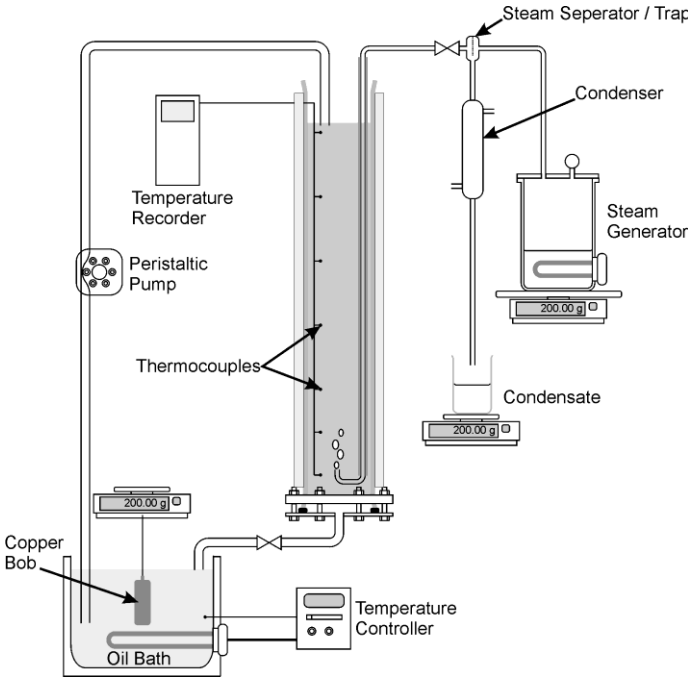

Figure 1 - Schematic of the experimental bubble column developed and used during this study

The temperature profile within the bubble column is measured by means of 7 type T thermocouples located at regular intervals along its length. These thermocouples which have an accuracy of ±0.8˚C are then connected to the temperature logging software. Upon start-up, the temperature within the bubble column is lower than in the oil bath. Thus the solution is allowed to circulate until no further changes in temperature are measured by any of the thermocouples (to within experimental accuracy of the thermocouples). At this point the system is assumed to have reached steady state.

A full factorial analysis involving three concentrations and temperatures was conducted. Three mass fractions (of lithium bromide salt) were selected. At each concentration, three different temperatures were then analysed. As the pressure of the system is to remain atmospheric, the temperatures selected for each concentration are limited by the saturation temperature of the solution. Thus for each concentration, temperatures were selected so that one is ~3.5˚C, one is ~10˚C, and one is ~15˚C below the saturation temperature for the solution. The resulting temperatures and concentrations used in the experiment are outlined in Table 1. In order to reference the different parameter settings succinctly, the concentrations and temperatures are named using levels as may be read from Table 1. Concentration levels run in ascending order from top to bottom and temperature levels in ascending order from left to right in Table 1. For example, Concentration 1-Temperature 2 means that this experimental run utilises a concentration of 46%(w/w) and a temperature of 119˚C.

Table 1 - All of the concentrations and temperatures used in the experiment

Concentration (%w/w)	Temperature (˚C)		
46	111	119	122
51	121	126	132
56	131	136	141

Saturated steam for the experiment was produced in a 53x25cm stainless steel cylindrical steam generator. The steam generated travels by insulated flexible tubing to the top of the cylinder. Condensed steam is prevented from entering the bubble column by making all steam flow through a steam trap, and the flowrate of steam entering the cylinder is controlled by means of a needle valve following this steam trap. Following the needle valve, the steam entering the bubble column is connected to a 2.15mm diameter stainless steel pipe (secured to the inside of the cylinder) through which it flows to the bottom of the cylinder. This pipe has a 180 degree bend at its submerged end, and thus acts as a sparger through which the steam bubbles are formed.

Upon start-up, a certain mass of air is contained within the steam generator. Therefore initially the needle valve controlling vapour flow into the bubble column is closed completely in order to ensure that as much air is removed from the system as feasible.

Two experimental runs were conducted for each concentration and temperature setting at different flowrates, with each experimental run lasting ten minutes. The bubbles were recorded using an AOS X-Motion high speed camera operating with a shutter speed of 500 frames per second. In order to ensure high visibility of the bubbles for the recordings, the bubble point of entry was illuminated using two Dedolight 150W Tungsten Aspherics spotlights and a Luxform 500W Halogen spotlight. The reflection of light off the bubble caused by these three spotlights ensures that there was sufficient contrast between the bubble and its surrounding fluid. Three recordings were taken during each experimental run at evenly spaced intervals.

Each recording was then analysed using the ProAnalyst Contour Tracking software package (Xcitex Inc.). This software was used to determine both the perimeter and projected area of each analysed bubble (in pixels). From each recording, three bubbles were selected at random (one from the beginning, one from the middle and one from the end of the recording) for analysis in order to ensure that representative results were obtained.

In order to determine the bubble's volume from the obtained perimeter and projected area, bubble sphericity is assumed. Thus using equation 2 an equivalent hydraulic diameter can be calculated which leads to a definition for the equivalent volume of the bubble given by equation 3.

$$D_{expt} := \frac{4A}{P} \qquad (2)$$

$$V_{expt} \coloneqq \frac{32\pi}{3}\left[\frac{A}{P}\right]^3 \quad (3)$$

All perimeter and projected area readings are recorded in pixels. The bubble is produced by the gas sparger, and thus these are (at least initially) located in the same plane relative to the camera. Therefore the width of the sparger is measured using a micrometer and compared to its width in pixels as recorded by the high speed camera. This allows for a conversion between pixels and length to be established which takes into consideration all refractive obstacles encountered by the light. This conversion ratio is measured for every single bubble analysed, as small movements of the camera or its refocusing may otherwise cause discrepancies.

MATHEMATICAL MODELLING

In the model, the bubble itself is being defined as the control volume of interest. The temperature of the bulk liquid in the system varies slightly over the length of the cylinder, but is shown to change negligibly with respect to time over the course of any one experimental run. The spatial distribution of temperature occurs gradually over the entire liquid height, however the vapour bubbles are found to absorb within the first few millimetres of contact liquid. Thus the temperature of the liquid is assumed to remain constant with respect to time at the average temperature as reported by the two closest thermocouples (on average within ~0.17% of each other).

Absorption Rate

Heat energy transfer in the liquid phase is assumed to occur by convection, and thus the overall energy balance at the site of absorption may be represented by equation 4.

$$Q_{abs} = k_v A_b \left.\frac{\partial T_v}{\partial r}\right|_{interface} + \alpha_L A_b (T_i - T_L) \quad (4)$$

Upon examination of the experimental data, it is observed that significant motion is occurring in the bubble which will result in a high degree of turbulence within the vapour phase and hence mixing. Due to this mixing and also the small diameter of the bubbles (~≤7mm), it was decided to simplify equation 4 further by assuming a uniform temperature within the bubble. Thus it is postulated that the interface temperature is very rapidly advected throughout the bubble, and therefore ($T_i \approx T_b$). Hence equation 4 may be reduced to equation 5.

$$Q_{abs} = \frac{\partial H_b}{\partial t} + \alpha_L A_b (T_b - T_L) \quad (5)$$

The heat of absorption is defined using a method similar to [13], utilising the partial specific enthalpy of water in the LiBr-H_2O solution (equation 6).

$$Q_{abs} = \frac{\partial m_v}{\partial t}\left[h_v(T_b, P_b) - h_{pw}(T_b, P_L, x_i)\right] \quad (6)$$

Thus the enthalpy balance across the vapour bubble is given by equation 7.

$$\frac{\partial H_b}{\partial t} = \frac{\partial m_v}{\partial t}\left[h_v(T_b, P_b) - h_{pw}(T_b, P_L, x_i)\right] - \alpha_L A_b (T_b - T_L) \quad (7)$$

Analogously to the heat transfer scenario, mass transfer across the bubble interface may be represented by equation 8. This equation examines the flow of water (not lithium bromide), and thus the term C corresponds to the concentration of water. However, as this study measures the mass fraction of lithium bromide experimentally (instead of water concentration), equation 8 is converted to equation 9 consisting of salt mass fraction terms.

$$\frac{\partial n_v}{\partial t} = -\beta_L A_b (C_i - C_L) \quad (8)$$

$$\frac{\partial m_v}{\partial t} = -\beta_L A_b \left((1 - x_i)\rho_i - (1 - x_L)\rho_L\right) \quad (9)$$

The effect of water inertia upon the collapse of the steam bubble is defined by the Rayleigh-Plesset equation shown in equation 10.

$$\frac{P_B(t) - P_L(t)}{\rho_L} = R_b \frac{d^2 R_b}{dt^2} + \frac{3}{2}\left(\frac{dR_b}{dt}\right)^2 + \frac{4\upsilon_L}{R_b}\frac{dR_b}{dt} + \frac{2\sigma}{\rho_L R_b} \quad (10)$$

Although this equation is derived based upon the assumption of a stationary spherical bubble, it is being used in this study, as it represents the limiting rate of bubble collapse (if heat and mass transfer were believed to occur extremely rapidly) and also approximates the relationship between the internal pressure of the vapour and the rate of change of its diameter.

Currently, three independent equations (equations 7, 9 and 10) have been derived, however four unknowns exist (T_b, x_i, P_b and R_b). Thus one further equation is required to provide closure. Saturation at the absorption interface is assumed to achieve this. As negligible pressure drop along the bubble's radial direction is also being assumed, the vapour pressure at the bubble interface must equal the pressure of the bubble (P_b). As a slight residue of air exists in the bubble, this should be accounted for in the vapour pressure model. The bubble is assumed to be saturated with water vapour, and thus we can estimate the partial pressure of water within the vapour (equation 11). The water-air mixture is treated as an ideal mixture, and thus Dalton's law is used to find the total pressure from the vapour volumetric fraction of water (equation 12).

$$P^v_{H_2O} = P^*_{LiBr}(T_b, x_i) \quad (11)$$

$$P_b = \left(\frac{1}{y_{H_2O}}\right) P^*_{LiBr}(T_b, x_i) = \left(\frac{1}{y_{H_2O}}\right) P^v_{H_2O} \quad (12)$$

Therefore equations 7, 9, 10 and 12 represent a set of interdependent, non-linear differential equations which characterise the absorption of a steam bubble in a LiBr-H_2O solution. These differential equations contain both liquid side heat and mass transfer coefficients (α and β respectively). These coefficients are calculated from the bubbles' Nusselt and Sherwood numbers using equations 13 and 14.

$$Nu = \frac{\alpha D}{k} \tag{13}$$

$$Sh = \frac{\beta D}{D_{ab}} \tag{14}$$

The correlations used to predict these Nusselt and Sherwood numbers are discussed as part of the Results section. It should be noted however that almost all of the sources from which the heat and mass transfer coefficient correlations are obtained define either a Nusselt or Sherwood number correlation, but not both. Thus the heat and mass transfer analogy is being implemented in this study, on the basis of analogous behaviour between heat and mass transfer.

Bubble Hydrodynamic Modelling

A simple model consisting of basic forces to describe the bubble vertical displacement versus time is developed. The forces included are buoyancy, weight, drag and added mass (or virtual mass). As the bulk solution is assumed to be quiescent in this model, the lift force is excluded in this section. The drag, weight and buoyancy forces are defined in equations 15 to 17.

$$F_D = -\frac{1}{2}\rho_L v_b^2 C_D A_{projected} \tag{15}$$

$$F_w = -\rho_v V_b g \tag{16}$$

$$F_B = \rho_L V_b g \tag{17}$$

As the surrounding fluid is assumed to be in a steady, isotropic state, the term Du/Dt = 0, and thus the virtual mass force expression used in this model may be simplified to equation 19.

$$F_{vm} = -\frac{\rho_L}{2}\left[V_b \frac{\partial v}{\partial t} + v\frac{\partial V_b}{\partial t}\right] \tag{18}$$

The final hydrodynamic model is given by equation 20.

$$m_b \frac{dv_b}{dt} = F_D + F_w + F_B + F_{vm} \tag{19}$$

RESULTS AND DISCUSSION

Experimental Results

The experimental results obtained highlight the speed at which the absorption of bubbles takes place. Unlike the simulation results reported by Merrill [9], the bubble diameter is not found to remain almost constant during the first 0.06 seconds of the absorption process. It may be seen that the majority of the absorption has been completed after 0.06 seconds in both Figures 2 and 3, while in Figure 4 the diameter has on average reduced by more than half its initial value at this point. In these three figures, the experimentally observed diameters from all of the experimental runs (at the particular temperature and concentration) are plotted against time. Absorption is found to be especially rapid at temperature level 1, while even at level 3 (~3.5˚C below the saturation temperature of the fluid) absorption occurs much more rapidly than has been previously achieved in any of the absorber studies cited in the introduction. The rapid absorptions depicted in Figures 2 to 4 represent a mass transfer coefficient of ~0.012m/s, which is therefore superior to the previous results outlined in the introduction by several orders of magnitude.

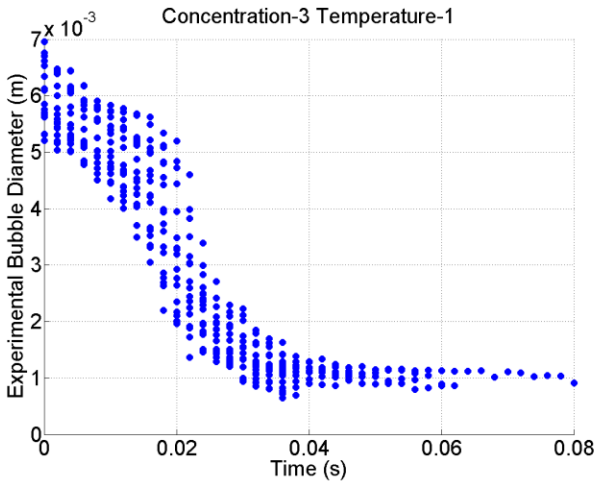

Figure 2 - Experimentally observed diameter versus time at concentration 3-temperature 1

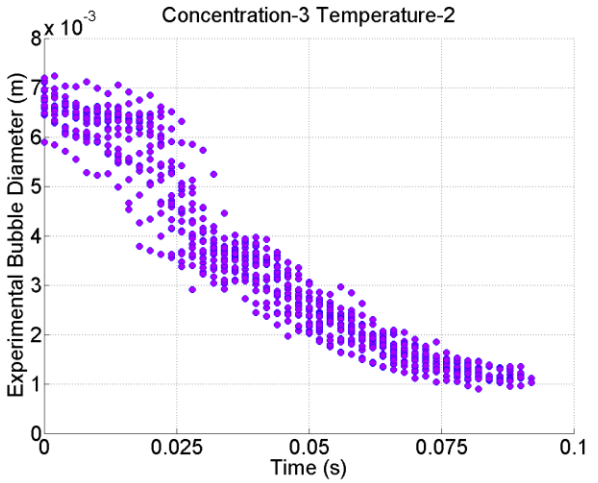

Figure 3 - Experimentally observed diameter versus time at concentration 3-temperature 2

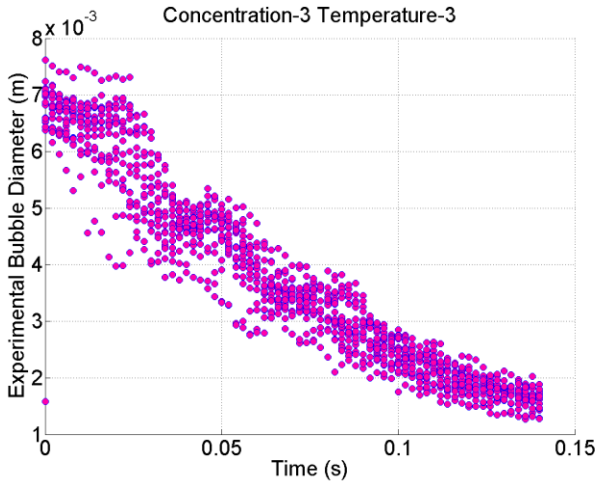

Figure 4 - Experimentally observed diameter versus time at concentration 3-temperature 3

Modelling Results

The set of non-linear differential equations developed in this paper describing the time dependent collapse of the steam bubble is dependent upon the inclusion of heat and mass transfer coefficients (α and β respectively). It is found that judicious selection of these parameters is of pivotal importance. From the experimental data, it is apparent that the bubbles are not perfectly spherical, and thus spherical correlations such as those developed by Azbel [14] dramatically underestimate the rate of absorption.

From analysis of the recorded data, it appears that the bubble collapse occurs in two distinct regimes or phases (apparent in Figure 2). In the first of these phases, the rate of absorption appears to be occurring relatively slowly, while the second phase shows a distinctly faster rate of collapse. The reason for this appears to be the onset of bubble shape deformation and bubble oscillation as illustrated in Figure 5. Thus in order to model these bubbles, Nusselt and Sherwood correlations are required which include such oscillations in their derivation.

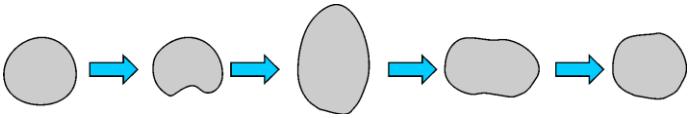

Figure 5 - Example of the oscillating nature of the bubble

The fresh surface model proposed by Clift [15] is used, in an attempt to include the effect of bubble oscillation in the simulation. As previously outlined, the heat and mass transfer analogy is used to convert the given Sherwood number equation to an equivalent Nusselt number correlation (equations 21 and 22).

$$Sh = \frac{2}{\sqrt{\pi}}\sqrt{\frac{D^2 f}{D_{ab}}}\sqrt{1+0.687\varepsilon} \qquad (20)$$

$$Nu = \frac{2}{\sqrt{\pi}}\sqrt{\frac{D^2 f}{\alpha_{therm}}}\sqrt{1+0.687\varepsilon} \qquad (21)$$

Bubbles entering the LiBr-H_2O solution are initially spherical but then begin to oscillate after a very short period of time. This spherical phase is however so short (~0.01 seconds) that it is approximated as being part of the oscillating regime in the model. In order to utilise the equations 21 and 22, two parameters, namely the frequency of oscillation (f) and the amplitude of the area oscillation (ε), need to be fixed. Clift [15] states that generally $\varepsilon \approx 0.3$, and thus this value is used in this study, while the value of f is approximated at 500Hz based upon the examination of recorded data. The relationship between the oscillating bubble model and observed experimental data is displayed in Figure 6.

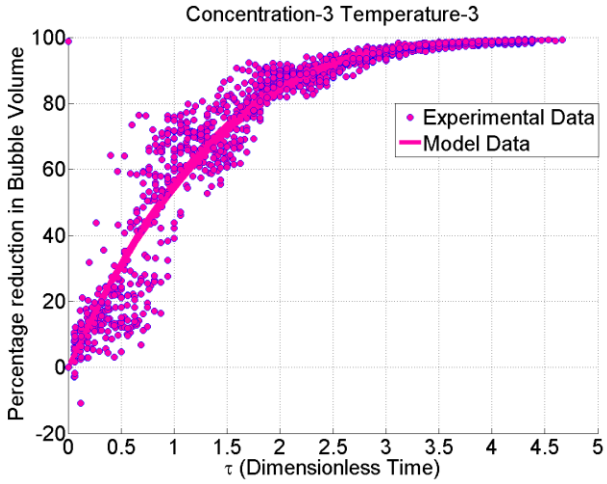

Figure 6 - Percentage reduction in bubble volume with respect to dimensionless time as predicted by the model and experimentally observed at concentration 3 and temperature 3

The model's goodness of fit it demonstrated in Figure 7. A slight over prediction of the absorption rate may be observed during the initial (spherical) phase of the bubble's residence time. However as reasoned previously, the time period over which this phase exists is so short that such over prediction has negligible effect upon the model's overall accuracy. Although a degree of scatter exists in the data (this is to be expected due to the inherent variability between different bubbles), the model achieves a coefficient of determination (R^2) of 0.96, indicating that it is capable of describing 96% of the observed experimental variance.

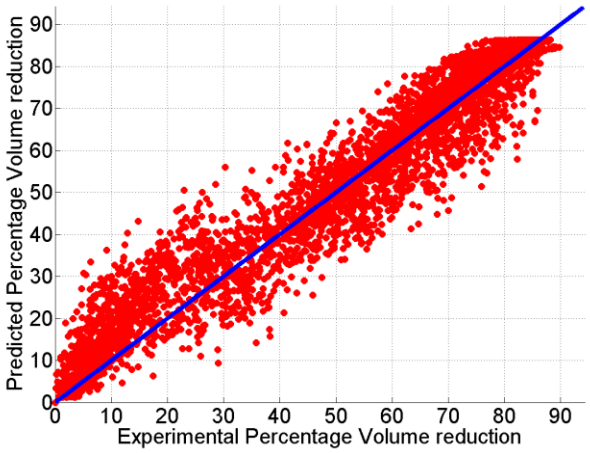

Figure 7 - Illustration of the goodness of fit between the model and the experimental data

CONCLUSION

An experimental analysis has been conducted, investigating the absorption of vapour bubbles in a concentrated lithium bromide (LiBr-H_2O) solution for use in the absorber of a heat transformer. An experimental bubble column is constructed and a high speed camera is used to track the collapse of the bubble. A model consisting of a set of nonlinear differential equations has been developed which is capable of describing this bubble collapse. It is determined that the Nusselt and Sherwood number correlations are highly significant factors in relating the model to observed data. A good fit is obtained with a fresh surface oscillating bubble model, capable of explaining 96% of all the experimentally observed variance. Mass transfer coefficients of 0.012m/s, represent a large increase upon values previously reported for other absorption methods, indicating that bubble absorption may be a highly efficient method of reducing the required size of this unit operation, and hence increasing the attractiveness of heat transformers.

ACKNOWLEDGEMENTS

Philip Donnellan would like to acknowledge the receipt of funding for this project from the Embark Initiative issued by the Irish Research Council. William Lee would also like to acknowledge the receipt of funding from the MACSI grant issued by Science Foundation Ireland (12/IA/1683).

REFERENCES

[1] P. Donnellan, *et al.*, "Internal energy and exergy recovery in high temperature application absorption heat transformers," *Applied Thermal Engineering*, vol. 56, pp. 1-10, 2013.

[2] P. Donnellan, *et al.*, "First and second law multidimensional analysis of a triple absorption heat transformer (TAHT)," *Applied Energy*, vol. 113, pp. 141-151, 2014.

[3] X. Ma, *et al.*, "Application of absorption heat transformer to recover waste heat from a synthetic rubber plant," *Applied Thermal Engineering*, vol. 23, pp. 797-806, 2003.

[4] P. Guo, *et al.*, "Energy and exergy analyses on the off-design performance of an absorption heat transformer," *Applied Thermal Engineering*, vol. 48, pp. 506-514, 2012.

[5] W. A. Miller and M. Keyhani, "The Correlation of Simultaneous Heat and Mass Transfer Experimental Data for Aqueous Lithium Bromide Vertical Falling Film Absorption," *Journal of Solar Energy Engineering*, vol. 123, pp. 30-42, 2000.

[6] F. S. K. Warnakulasuriya and W. M. Worek, "Drop formation of swirl-jet nozzles with high viscous solution in vacuum-new absorbent in spray absorption refrigeration," *International Journal of Heat and Mass Transfer*, vol. 51, pp. 3362-3368, 2008.

[7] D. Arzoz, *et al.*, "Experimental study on the adiabatic absorption of water vapor into LiBr–H2O solutions," *Applied Thermal Engineering*, vol. 25, pp. 797-811, 2005.

[8] E. Palacios, *et al.*, "Lithium bromide absorption machines: Pressure drop and mass transfer in solutions conical sheets," *Energy Conversion and Management*, vol. 50, pp. 1802-1809, 2009.

[9] T. L. Merrill and H. Perez-Blanco, "Combined heat and mass transfer during bubble absorption in binary solutions," *International Journal of Heat and Mass Transfer*, vol. 40, pp. 589-603, 1997.

[10] J. Castro, *et al.*, "Comparison of the performance of falling film and bubble absorbers for air-cooled absorption systems," *International Journal of Thermal Sciences*, vol. 48, pp. 1355-1366, 2009.

[11] K. Abrahamsson, *et al.*, "Application of heat pump systems for energy conservation in paper drying," *International Journal of Energy Research*, vol. 21, pp. 631-642, 1997.

[12] S. V. Stankus, *et al.*, "The density of aqueous solutions of lithium bromide at high

temperatures and concentrations," *High Temperature,* vol. 45, pp. 429-431, 2007.

[13] M. Raisul Islam, *et al.*, "Simplified models for coupled heat and mass transfer in falling-film absorbers," *International Journal of Heat and Mass Transfer,* vol. 47, pp. 395-406, 2004.

[14] D. Azbel and P. Kemp-Pritchard, *Two-phase Flows in Chemical Engineering*: Cambridge University Press, 1981.

[15] R. Clift, *et al.*, *Bubbles, Drops, and Particles*. New York: Academic Press Inc., 1978.